PROCEEDINGS OF SCIENCE

Optimizing Material Selection and Operational Conditions for XHV Systems: Lessons from AISI 1020 and 316L Comparative Studies

Aiman H. Al-Allaq [a]*, Md Abdullah Mamun [b], Matt Poelker [b] and Abdelmageed Elmustafa [a]

[a] *Old Dominion University, 5115 Hampton Blvd, Norfolk, VA 23529, USA*

[b] *Jefferson Lab, 12000 Jefferson Ave, Newport News, VA 23606, USA*

E-mail: aalal005@odu.edu

In this study, AISI 1020 low-carbon steel was investigated as a cost-effective alternative to SS316L stainless steel for reaching extreme high vacuum (XHV) conditions. After being baked at 400 °C, a vacuum chamber made of low-carbon steel material exhibited an outgassing rate approximately 2000 times smaller than a similar chamber made of stainless steel. Its activation energy for hydrogen diffusion (27.00 kJ/mol) is less than half that of stainless steel (60.30 kJ/mol), indicating more efficient hydrogen removal during bakeout. MolFlow+ simulations supported the experimental data and demonstrated the importance of system geometry optimization and minimizing stainless steel content for achieving optimal vacuum performance. AISI 1020's magnetic properties, typically considered disadvantageous for accelerator applications, could benefit spin-polarized electron sources by shielding photocathodes from stray fields while simultaneously providing improved vacuum through reduced outgassing. To optimize AISI 1020's performance in XHV systems, practical considerations include pre-baking protocols and careful system design to minimize stainless steel components.

20th International Workshop on Polarized Source, Targets, and Polarimetry (PSTP2024)
22-27 September 2024
Jefferson Lab, Newport News, VA

* Speaker

ISSN 1824-8039 . Published by SISSA Medialab.

PoS(PSTP2024)070

1. Introduction

Today's state-of-the-art spin-polarized photoelectron guns operate in the ultrahigh vacuum regime at pressures around 10^{-12} Torr, which limits beam delivery duration and maximum achievable currents [1,2]. While stainless steel materials such as AISI 316L are widely used for vacuum systems due to their strength and corrosion resistance, they come with challenges - particularly hydrogen outgassing, which can limit the achievable vacuum and increase pre-treatment costs. For heat treatment of stainless steel at temperatures between 150 °C and 250 °C (bake duration ~48 hours), published literature shows general consensus: one can expect hydrogen outgassing rates in the range of 10^{-12} Torr L/s/cm². However, reports of outgassing rate reduction following 400 °C bakeout show considerable variation, with improvement factors ranging from 10 to 500 [3–6]. At Jefferson Lab, where considerable effort has been made to minimize outgassing, heat treatments of stainless steel performed under vacuum at 400 °C for 48-100 hours typically reduce outgassing by factors of 10-20, yielding rates in the range of 10^{-13} Torr L/s/cm² [4]. These variations in reported outgassing rates highlight the challenges of achieving and maintaining extreme high vacuum conditions using stainless steel chambers.

AISI 1020 low-carbon steel has emerged as a promising alternative for XHV applications. Our measurements demonstrate that AISI 1020 low-carbon steel can achieve hydrogen outgassing rates approximately 2000 times lower than AISI 316L after heat treatment at 400 °C, with rates reaching as low as 2.35×10^{-16} Torr L/s/cm² [7]. This dramatic improvement surpasses previously reported results for similar materials, which range from 4.70×10^{-14} to 3.10×10^{-13} Torr L/s/cm² [5] and 4.40×10^{-15} to 1.30×10^{-14} Torr L/s/cm² [8]. This improved vacuum performance could enable longer uninterrupted beam delivery and higher beam currents than achieved today, which is critical for the development of polarized positron sources [9,10].

Typically, low-carbon steel is not considered for accelerator application because it is magnetic. But for spin-polarized beam applications, this could serve as an advantage by shielding photocathodes from stray magnetic fields in polarized electron sources, thereby enhancing beam stability [8].

While low-carbon steel shows promise for XHV applications, its integration requires careful preparation. Surface contaminants must be removed through acid etching and pre-baking, and high-temperature exposure can lead to magnetite formation, affecting outgassing performance [11–16]. Moreover, the pressure achieved inside a photogun is not solely dependent on the outgassing properties of the photogun vacuum chamber: a photogun includes the ceramic insulator, the photogun electrodes which might be made of stainless steel, and components like valves which undoubtedly will be made of stainless steel, and there is the connection to the accelerator beamline. In our test setup, stainless steel components contributed approximately 5% of the total surface area, and MolFlow+ simulations suggest that reducing this contribution to below 1% could enable pressures in the 10^{-13} Torr range [17,18].

This article examines the system-level improvements needed to optimize low-carbon steel for XHV applications. To compare the performance of low carbon and stainless steels under various vacuum conditions, we employed experimental measurements using ion pumps (25 L/s N_2) and NEG pumps (50 L/s H_2), MolFlow+ simulations, and surface science evaluations. Surface contamination, oxidation effects, and mixed-material considerations significantly impact vacuum performance [3,5,15,16]. Understanding these challenges is crucial for optimizing both material behavior and system design.

2. Design and Experimental Approach

This experimental study utilized vacuum chambers constructed from 122 cm long tubes with 6.35 cm outer diameter, compatible with standard DN63 Conflat flanges. Test chambers were fabricated from both AISI 1020 low-carbon steel and 316L stainless steel, with the 1020 tubes featuring thicker walls (4.4 and 5.7 mm) compared to their stainless-steel counterparts (0.5 and 1.0 mm).

Material preparation proved critical for achieving optimal vacuum performance. The as-received 1020 tubes exhibited significant surface contamination requiring rigorous cleaning protocols. The cleaning procedure involved immersing the tubes in hydrochloric acid diluted with deionized water to achieve 18.25-19% HCl concentration. After approximately one minute of etching, the tubes were immediately rinsed with deionized water, followed by acetone, and dried using filtered nitrogen gas. The tubes were then sealed in clean room bags with nitrogen backfill until assembly. For comparison, stainless steel components underwent standard ultrasonic cleaning in mild alkaline detergent. However, previous studies have shown that different surface treatments, such as acid etching, electrochemical polishing, and hydrogen treatment, can significantly alter the outgassing characteristics of stainless steel by reducing the desorption of water and CO/N_2 [19]. Research has demonstrated that electrochemical polishing and dissociated hydrogen gas treatment result in lower desorption rates compared to conventional detergent-based cleaning, suggesting that the choice of surface preparation method plays a critical role in outgassing behavior [19].

Two distinct configurations were employed, as described below. In both configurations, Conflat end flanges were made of 316L stainless steel. For the chambers made of low-carbon steel, these end flanges were vacuum degassed at 400 °C for 48 hours before welding to minimize their outgassing contribution. For the low-carbon steel chambers, stainless steel components contributed approximately 5% of the total vacuum-exposed surface area.

3. Results

3.1 Hydrogen Outgassing Rates and Activation Energy

The first setup utilized the accumulation method (rate-of-rise) following American Vacuum Society recommendations [20,21]. As illustrated in Figure 1, a schematic of the outgassing rate measurement setup is shown in Figure 1, employing a spinning rotor gauge (SRG) to monitor pressure changes after isolating the chamber from the turbomolecular pump system. The outgassing rate q was calculated using:

$$q = (\Delta P/\Delta t)\times(V/A)\ \text{Torr L/s/cm}^2 \qquad \text{Eq. 1}$$

where V is the chamber volume, A is the surface area, and $\Delta P/\Delta t$ represents the pressure rise rate. The SRG was programmed to measure hydrogen (mass 2) pressure directly.

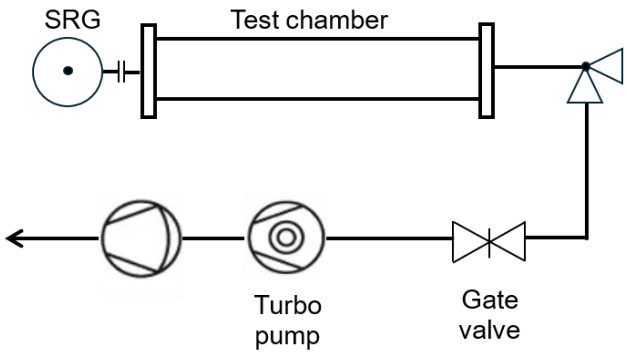

Figure 1: A schematic of the H_2 outgassing rate measurement setup.

To evaluate reproducibility and treatment effects, we tested two chambers of each material. The first stainless steel chamber (designated 316L#1) was tested without pre-treatment, while the second (316L#2) underwent vacuum degassing at 400 °C for 24 hours prior to testing. Similarly, we prepared two low-carbon steel chambers (1020#1 and 1020#2) to investigate different heat treatment protocols.

The hydrogen outgassing measurements for stainless steel chambers provided essential benchmarking of our experimental setup. The untreated 316L#1 chamber exhibited an outgassing rate of 5.75×10^{-12} Torr L/s/cm² following bakeout at 150 °C. Pre-baking 316L#2 at 400 °C for 24 hours reduced the outgassing rate to 5.60×10^{-13} Torr L/s/cm², demonstrating the effectiveness of thermal treatment. While this reduction is smaller than some reports in the literature, it aligns well with previous measurements at Jefferson Lab, where 400 °C treatments typically reduce hydrogen outgassing by factors of 10-20, yielding rates in the 10^{-13} Torr L/s/cm² range.

The 1020 low-carbon steel results proved particularly noteworthy. Without pre-baking, 1020#1 achieved an outgassing rate of 3.90×10^{-13} Torr L/s/cm² after just 150 °C bakeout - matching the performance of 316L#2 after 400 °C treatment. Even more remarkable was the dramatic reduction seen in 1020#2 after 400 °C bakeout, reaching 2.40×10^{-16} Torr L/s/cm². This represents a 2000-fold improvement over similarly treated stainless steel.

Previous studies of low-carbon steel have reported outgassing rates ranging from 4.4×10^{-15} to 1.30×10^{-14} Torr L/s/cm² following bakeout at 80 °C [8], and 4.70×10^{-14} to 3.10×10^{-13} Torr L/s/cm² after 150 °C treatment [5]. Our result following 400 °C treatment represents the lowest reported hydrogen outgassing rate for this class of materials as shown in Figure 2. Notably, these measurements were not corrected for gas contributions from the stainless steel components integral to the assembled apparatus [7].

Analysis of the temperature-dependent outgassing behavior revealed significantly different activation energies for hydrogen diffusion in the two materials. The low carbon steel exhibited an activation energy of 27.0 kJ/mol, less than half that measured for stainless steel (60.3 kJ/mol). This lower activation energy indicates more efficient hydrogen removal during bakeout, consistent with the observed improvements in outgassing performance.

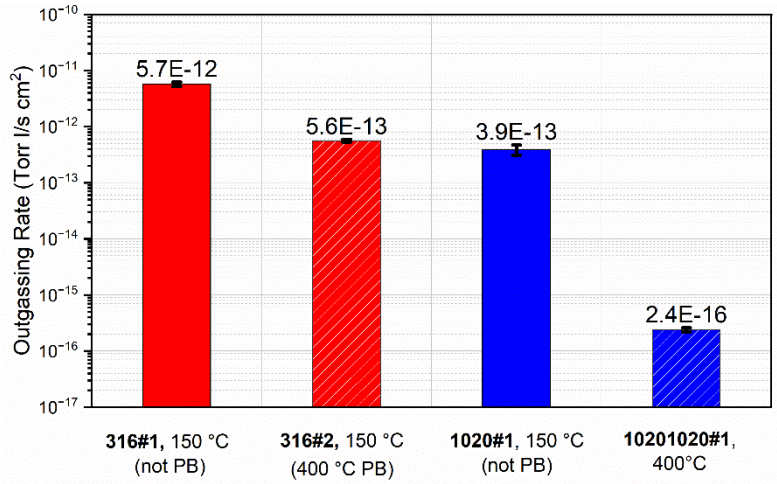

Figure 2: Comparison of hydrogen outgassing behavior for AISI 316L stainless steel (left) and AISI 1020 low-carbon steel (right) measured at room temperature following various heat treatments.

3.2 Ultimate Pressure Measurements

The second configuration focused on achieving minimum pressure using a combined pumping approach. As shown in Figure 3, this setup employed:

- An ion pump (nominal 25 L/s N_2 pump speed)
- A non-evaporable getter pump (nominal 50 L/s H_2)
- A bakeable all-metal gate valve for pump isolation
- An extractor gauge for accurate pressure measurement

Chambers were initially evacuated using a turbomolecular pump to approximately 1.00×10^{-8} Torr before transitioning to the ion/NEG pump combination. The NEG pump was activated per manufacturer specifications, with liberated gases removed via the turbopump. A LabVIEW-based system monitored pressure and temperature throughout testing.

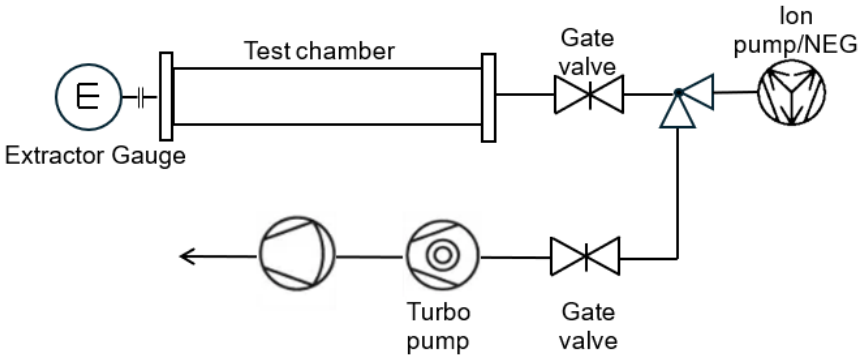

Figure 3: Setup for ultimate pressure measurement.

The ultimate pressure (P_{ult}) in a vacuum system is governed by the balance between outgassing rate (q) and effective pumping speed (S):

$$P_{ult} = qA/S \qquad \text{Eq. 2}$$

where A is the chamber surface area. This relationship directly connects lower outgassing rates to improved vacuum performance.

Ultimate pressure measurements confirmed that 1020 outperformed 316L under identical conditions. The system achieved pressures as low as 1.00×10^{-11} Torr after a 250 °C bake, approximately 10 times lower than 316L's best performance of 8.60×10^{-11} Torr after 400 °C bake, as shown in Figure 4. However, an unexpected observation emerged at higher temperatures: 400 °C bakeout of the 1020 system resulted in slightly degraded vacuum performance compared to the 250 °C treatment. This performance degradation at elevated temperatures correlates with significant surface oxidation of the low-carbon steel, as discussed below. This uncontrolled oxide formation at higher temperatures likely contributes to the observed vacuum performance limitations [15,16].

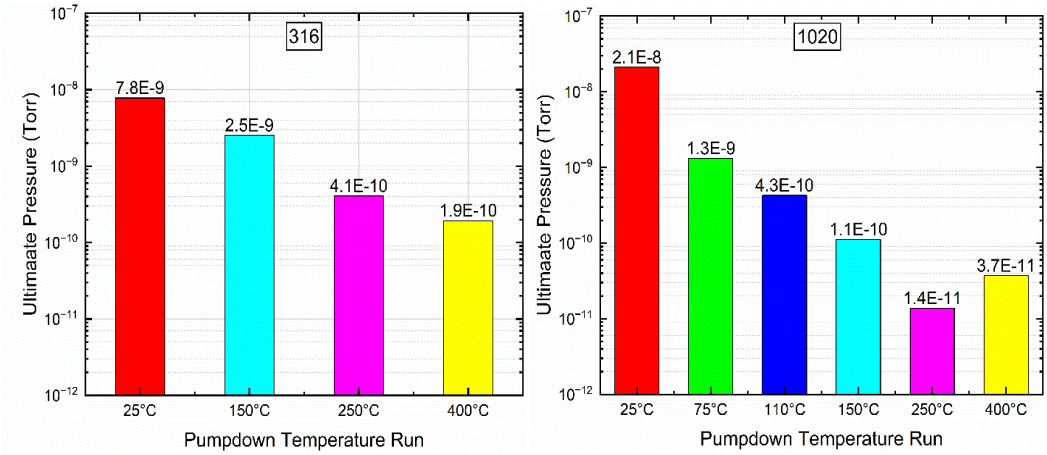

Figure 4: Ultimate pressure achieved at room temperature after 100 hours of NEG/ion pump operation, plotted versus the temperature of prior heat treatment for (right) 1020 and (left) 316L chambers.

3.3 MolFlow+ Simulations

Our experimental measurements revealed distinct outgassing characteristics between 1020 and 316L chambers. While the 1020 low-carbon steel exhibited an outgassing rate 2000 times lower than 316L after 400 °C treatment (2.35×10^{-16} vs 5.75×10^{-12} Torr L/s/cm²), the ultimate pressure improved by only a factor of 10. MolFlow+ simulations helped explain this apparent discrepancy and identify paths to better performance.

Simulations were first performed using measured outgassing rates for 316L stainless steel (2.00×10^{-12} to 5.00×10^{-12} Torr L/s/cm²) to estimate the pump speed at the location of the extractor gauge. When the pump speed at the location of the extractor gauge was set to values between 28 and 35 L/s, the simulation accurately predicted the measured pressures on both sides of the vacuum system as shown in Figure 5 (left). These pump speed values align well with the conductance calculation using the formula for molecular flow through a long tube, which predicts ~27 L/s for our geometry.

Next, using these validated pump speeds, simulations were performed for the low-carbon steel vacuum chamber. When outgassing rates were set to values between 1.00×10^{-16} and 6.00×10^{-16} Torr L/s/cm², the simulation predicted the pressures that were measured on both sides of the

vacuum apparatus (Figure 5, right). Importantly, this range of outgassing rate is consistent with the measured values noted above.

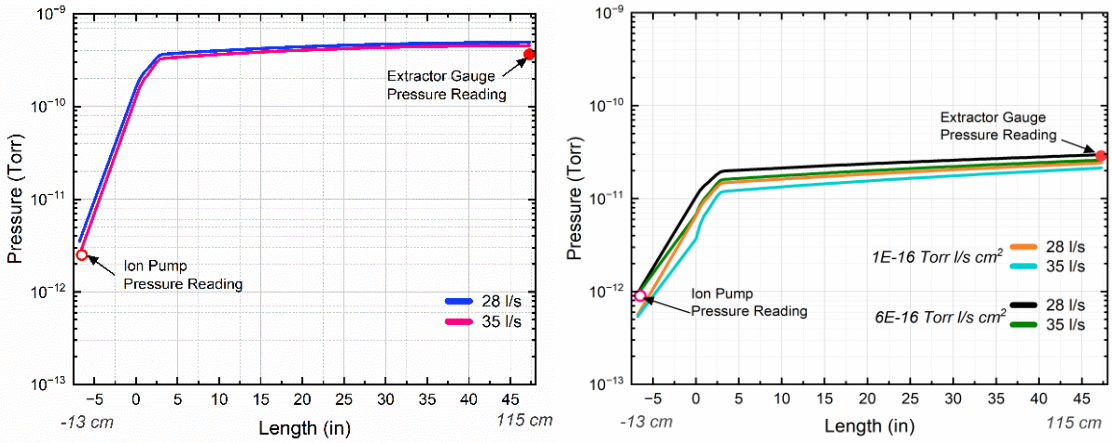

Figure 5: Molflow+ simulation results - pressure profiles along the length of the tube-shaped vacuum apparatus: (left) The simulation accurately predicts measured pressure at both ends of the stainless-steel apparatus when pump speed was set to values between 28 and 35 L/s at the location of the extractor gauge, (right) simulations predict the measured pressure at both ends of the AISI 1020 low-carbon steel system when outgassing rates were set to values within the range of 1.00×10^{-16} to 6.00×10^{-16} Torr L/s/cm². This range is consistent with measured values.

Most significantly, the simulations revealed that stainless steel components, despite comprising only 5% of the total surface area, created localized pressure gradients that limited overall system performance. As shown in Figure 6, reducing stainless steel content below 1% could enable pressures in the 10^{-13} Torr range. This finding has important implications for photogun design - components traditionally made of stainless steel, particularly the electrodes, would need to be fabricated from low-carbon steel to achieve optimal performance [1,2,22].

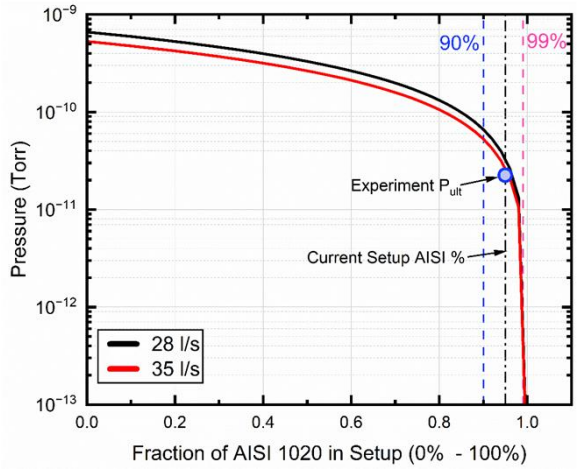

Figure 6: Predictions of ultimate pressure versus stainless steel surface area fraction for pump speeds of 28 L/s (black line) and 35 L/s (red line). The experimental data point (blue circle) represents our current setup with ~5% stainless steel contribution. Vertical dashed lines indicate 90% and 99% low-carbon steel composition thresholds.

4. Surface Oxidation and Its Effect on Vacuum Performance

Understanding surface transformations in AISI 1020 low-carbon steel under various heat treatments proved crucial for optimizing vacuum performance. Test coupons (5 mm^2 surface area, 2.7 mm thickness) prepared from similar 1020 stock underwent similar heat treatment followed by systematic characterization using energy-dispersive X-ray spectroscopy (EDS), scanning electron microscopy (SEM), and atomic force microscopy (AFM).

Surface analysis revealed distinct oxidation stages correlated with vacuum performance. As shown in Figure 7, SEM imaging demonstrates the dramatic evolution of surface morphology with temperature. At 250 °C, the oxide film consists of laterally spread colonies with layered structure, suggesting a magnetite-rich composition. This treatment temperature coincided with optimal vacuum performance. At 400 °C, larger swollen oxide grains indicate extensive oxidation and growth, corresponding to slightly degraded vacuum performance compared to 250 °C treatment. For comparison, a steam-treated reference sample exhibits a distinctly different columnar oxide structure with vertical grain orientation.

Quantitative surface characterization revealed systematic evolution with temperature treatment, as shown in Figure 8. Surface roughness increased from approximately 4 nm at 75 °C to 21 nm at 400 °C, while grain size grew from 15 nm to 78 nm over the same temperature range. The crystallite size of the magnetite phase also demonstrated significant growth, increasing from 18 nm at 250 °C to 42 nm at 400 °C. This crystallite growth correlated with increased oxygen content, which jumped dramatically from 2.40% at 250 °C to 30.60% at 400 °C.

XRD and EDS analyses provided complementary evidence for oxide formation and composition changes, as shown in Figure 9. At temperatures above 250 °C, distinct diffraction peaks characteristic of magnetite (Fe_3O_4) and hematite (α-Fe_2O_3) phases emerged. The oxygen content showed a corresponding increase with temperature: from 1.73% at 150 °C to 2.40% at 250 °C, followed by a substantial rise to 30.64% at 400 °C. The steam-treated reference sample showed the most pronounced oxide peaks, confirming the successful formation of a thick oxide layer.

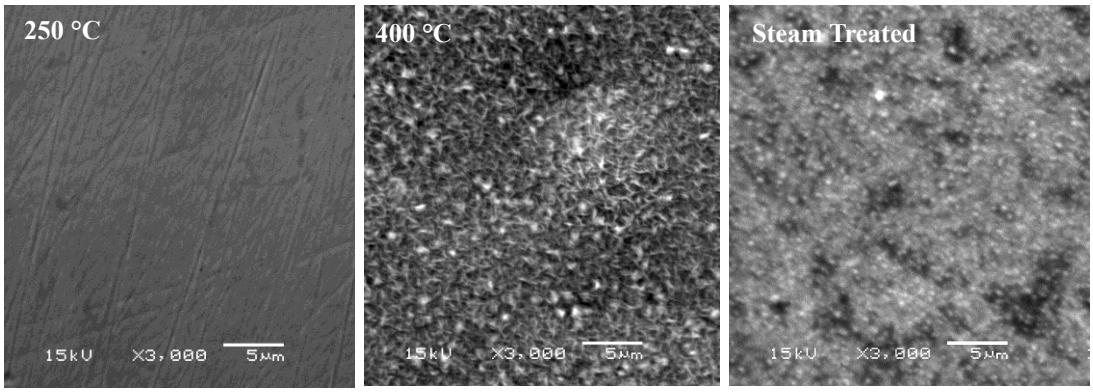

Figure 7: SEM images comparing surface morphology of 1020 coupons treated at 250 °C (top), 400 °C (middle), and steam-treated reference sample (bottom).

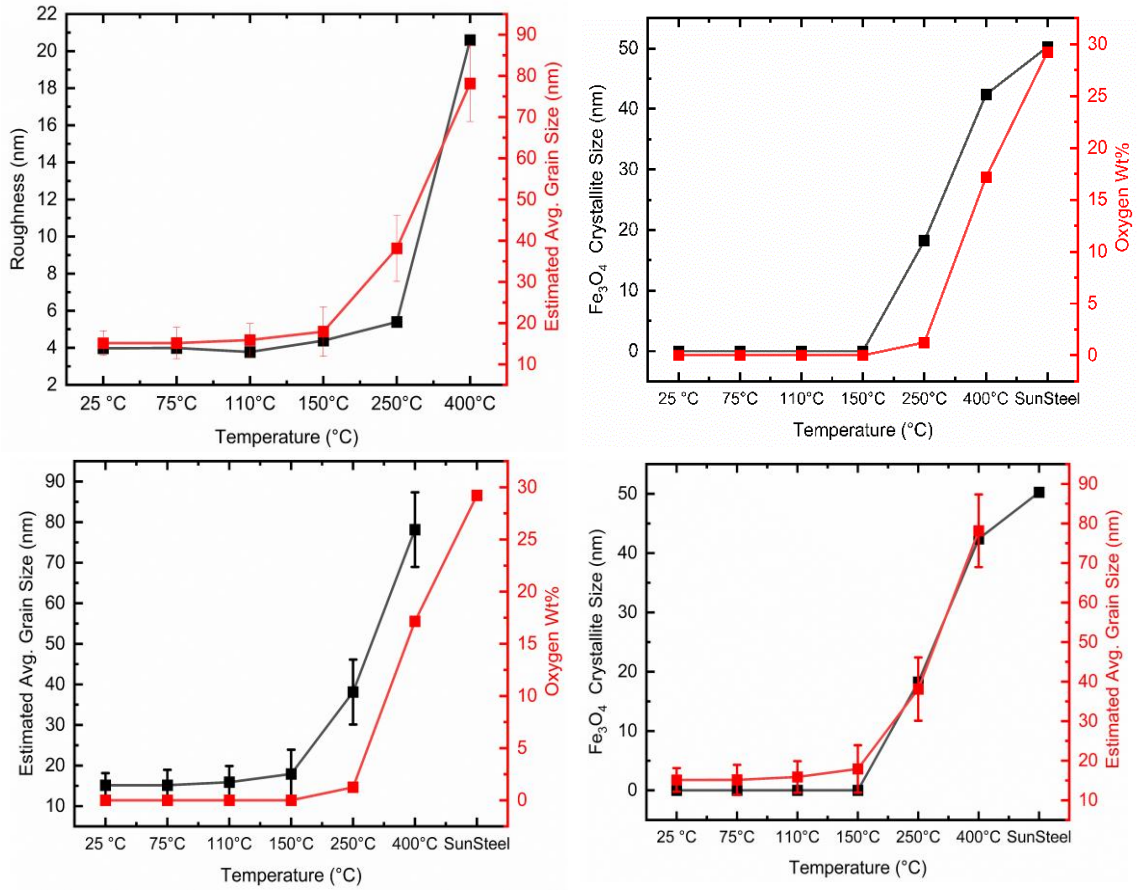

Figure 8: Evolution of surface properties with temperature: (a) Surface roughness and grain size, (b) Fe_3O_4 crystallite size and oxygen content, demonstrating systematic surface transformation with increasing temperature.

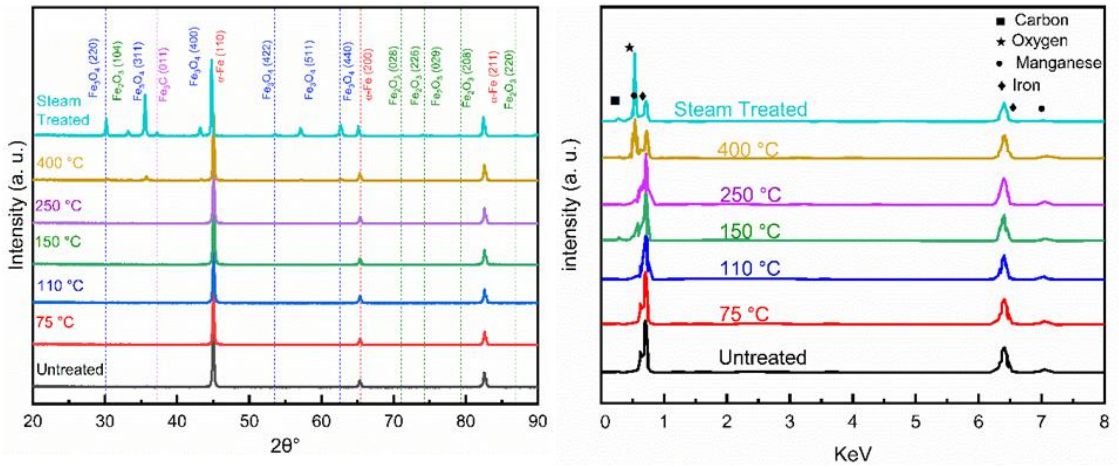

Figure 9: (a) XRD patterns and (b) EDS spectra of 1020 coupons subjected to various heat treatments, showing progressive oxide formation and increased oxygen incorporation.

5. Conclusions

This study demonstrates low-carbon steel's potential as a cost-effective alternative to stainless steel for extreme high vacuum (XHV) applications. The remarkable reduction in hydrogen outgassing ~2000 times lower than 316L after 400 °C bakeout - establishes 1020's viability for achieving pressures in the XHV regime. However, our findings emphasize that while the outgassing rate of 1020 can reach 2.35×10^{-16} Torr L/s/cm², achieving optimal system performance requires careful attention to mixed-material effects, as untreated stainless-steel components can significantly impact overall vacuum achievement.

Surface oxidation studies on test coupons made of AISI 1020 low-carbon steel revealed the formation of magnetite (Fe_3O_4) and hematite (α-Fe_2O_3) at elevated temperatures, with complex implications for vacuum performance. While controlled oxide formation appears beneficial up to 250 °C, extensive oxidation at 400 °C correlates with slightly degraded vacuum performance. Surface analyses demonstrated systematic evolution of roughness, grain size, and oxide composition with temperature, providing insight into optimal processing conditions.

To quantify potential benefits for actual photogun systems, we calculated achievable pressures using P = qA/S for the CEBAF photogun geometry (surface area A = 9230.95 cm²) across a range of pump speeds, as shown in Figure 10. The present CEBAF 200 kV DC high voltage photogun employs six NEG modules providing approximately ~ 8000 L/s total pump speed (indicated by vertical dashed lines). At this pump speed, today's stainless-steel system with outgassing rates of 10^{-12} to 10^{-13} Torr L/s/cm² should reach pressures in the low 10^{-12} - 10^{-13} Torr range. Pressure measurements made using a similar photogun vacuum chamber corroborate these values [23]. For a new photogun made using low-carbon steel and employing the same NEG pump array, the simple expression noted above indicates the pressure within the photogun could reach into the 10^{-16} Torr range. But this implies everything within the photogun be made of low-carbon steel, which might not be possible. For example, a reliable photogun must employ a cathode electrode that produces no field emission when biased at high voltage. It is unknown if low-carbon steel represents viable material for manufacturing electrodes: field emission studies of electrodes made from low-carbon steel represents an important next step. In addition, the adjacent beamline made of stainless steel could represent a significant gas load into the photogun. Detailed MolFlow+ simulations are warranted to optimize the photogun-to-beamline connection.

Although much work remains, the insights from this work suggest that significant improvements in XHV system performance and cost-effectiveness are achievable through the strategic use of low-carbon steel when proper design considerations are implemented.

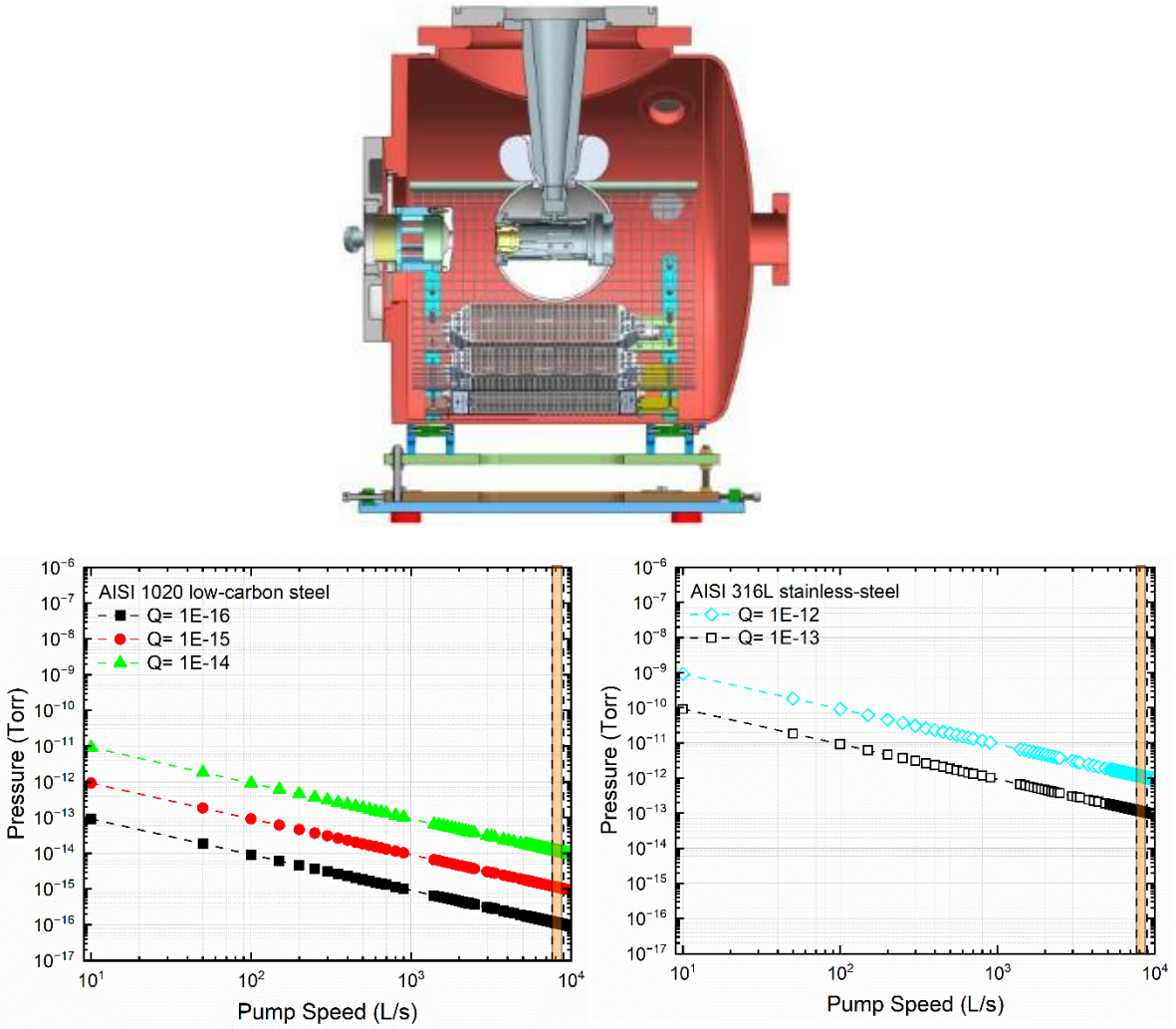

Figure 10: (top) Cutaway view of the CEBAF 200 kV DC high voltage spin polarized photogun, (bottom right) Calculated ultimate pressure versus pump speed for various outgassing rates, using actual CEBAF photogun surface area. (bottom left) The curves demonstrate potential vacuum improvement through systematic reduction in the outgassing rate from 10^{-13} to 10^{-16} Torr L/s/cm².

Acknowledgments

The authors are grateful for the advice and many helpful suggestions from the Gravity Wave Observatory Working Group, including many conversations with local colleagues at The College of William and Mary. The authors wish to thank Marcy Stutzman, Steve Covert, and Joseph J. Maniscalco for assistance related to setting up the experiment, troubleshooting problems with data acquisition, and LabView programming. This material is based upon work supported by the U.S. Department of Energy, Office of Science, Office of Nuclear Physics under contract DE-AC05-06OR23177.

References

[1] Grames J, Suleiman R, Adderley P A, Clark J, Hansknecht J, Machie D, Poelker M and Stutzman M L 2011 Charge and fluence lifetime measurements of a dc high voltage GaAs photogun at high average current *Physical Review Special Topics - Accelerators and Beams* **14** 43501

[2] Stutzman M L, Adderley P, Brittian J, Clark J, Grames J, Hansknecht J, Myneni G R and Poelker M 2007 Characterization of the CEBAF 100kV DC GaAs photoelectron gun vacuum system *Nucl Instrum Methods Phys Res A* **574** 213–20

[3] Dylla H F, Manos D M and LaMarche P H 1993 Correlation of outgassing of stainless steel and aluminum with various surface treatments *Journal of Vacuum Science & Technology A* **11** 2623–36

[4] Mamun M A A, Elmustafa A A, Stutzman M L, Adderley P A and Poelker M 2013 Effect of heat treatments and coatings on the outgassing rate of stainless steel chambers *Journal of Vacuum Science & Technology A* **32** 021604

[5] Park C, Ha T and Cho B 2015 Thermal outgassing rates of low-carbon steels *Journal of Vacuum Science & Technology A* **34** 021601

[6] Park C D, Chung S M, Liu X and Li Y 2008 Reduction in hydrogen outgassing from stainless steels by a medium-temperature heat treatment *Journal of Vacuum Science & Technology A* **26** 1166–71

[7] Al-Allaq A H, Mamun M A, Poelker M and Elmustafa A 2025 *A side-by-side evaluation of the outgassing rate and ultimate pressure achieved inside tubes made of low-carbon and stainless steel* (Newport News)

[8] Scarcia C, Bregliozzi G, Chiggiato P, Ingrid Michet A, Perez Fontenla A T, Rimoldi M, Taborelli M and Wevers I 2024 Study of selected mild steels for application in vacuum systems of future gravitational wave detectors *Journal of Vacuum Science & Technology B* **42**

[9] Musumeci P, Boffo C, Bulanov S S, Chaikovska I, Golfe A F, Gessner S, Grames J, Hessami R, Ivanyushenkov Y and Lankford A 2022 Positron sources for future high energy physics colliders *arXiv preprint arXiv:2204.13245*

[10] Kazimi R, Grames J, Hofler A, Hernandez-Garcia C and Palacios Serrano G 2023 Polarized electron injector for positron production at CEBAF (United States)

[11] Mattox D M 1998 Preparation and cleaning of vacuum surfaces *Handbook of Vacuum Science and Technology* (Elsevier) pp 553–606

[12] Luo Y, Wu X, Wang K and Wang Y 2020 Comparative study on surface influence to outgassing performance of aluminum alloy *Appl Surf Sci* **502** 144166

[13] Dylla H F, Manos D M and LaMarche P H 1993 Correlation of outgassing of stainless steel and aluminum with various surface treatments *Journal of Vacuum Science & Technology A: Vacuum, Surfaces, and Films* **11** 2623–36

[14] He P, Hseuh H C, Mapes M, Todd R, Weiss D and Wilson D 2003 Hydrogen Outgassing and Surface Properties of TiN-Coated Stainless Steel Chambers *AIP Conf Proc* **671** 292–9

[15] Ishikawa Y, Yoshimura T and Ozaki T 1991 Adsorption of water on the iron surface with reference to corrosion *Zairyo-to-Kankyo* **40** 540–4

[16] ISHIKAWA Y 1997 Adsorption and desorption of water molecules on the surface of vacuum materials *Shinku* **40** 145–7

[17] Yamanaka S, Watanabe H and Okushi H 2000 Adsorption isotherms *Appl Surf Sci* **159** 611–34

[18] Kersevan R and Pons J-L 2009 Introduction to MOLFLOW+: New graphical processing unit-based Monte Carlo code for simulating molecular flows and for calculating angular coefficients in the compute unified device architecture environment *Journal of Vacuum Science & Technology A* **27** 1017–23

[19] Shin Y H, Lee K J and Jhung K C 1996 Study of outgassing of stainless steel with various surface treatments *Vacuum* **47** 679–82

[20] Redhead P A 1993 Uhv and xhv pressure measurements *Vacuum* **44** 559–64

[21] Redhead P A 2002 Recommended practices for measuring and reporting outgassing data *Journal of Vacuum Science & Technology A* **20** 1667–75

[22] Mamun M A, Adderley P A, Benesch J F, Bullard D B, Delayen J R, Grames J M, Guo J, Hannon F E, Hansknecht J, Hernandez-Garcia C, Kazimi R, Krafft G A, Poelker M, Suleiman R, Tiefenback M G, Wang Y W, Wijethunga S A K and Zhang S 2018 Production of Magnetized Electron Beam from a DC High Voltage Photogun *International Particle Accelerator Conference* 9 ed S Koscielniak, T Satogata, V R W Schaa and J Thomson (JACoW Publishing) pp 4567–70

[23] Stutzman M L, Adderley P A, Mamun M A A and Poelker M 2018 Nonevaporable getter coating chambers for extreme high vacuum *Journal of Vacuum Science & Technology A* **36** 31603